

Steering a Historical Disease Forecasting Model Under a Pandemic: Case of Flu and COVID-19

Alexander Rodriguez^{*§}, Nikhil Muralidhar^{†§}, Bijaya Adhikari[‡], Anika Tabassum^{*†},
Naren Ramakrishnan[†], B. Aditya Prakash^{*}

^{*}College of Computing, Georgia Institute of Technology, Atlanta, USA

[†]Department of Computer Science, Virginia Tech, Arlington, USA

[‡]Department of Computer Science, University of Iowa, Iowa City, USA

{arodriguezc, badityap}@gatech.edu, {nik90, anikat1, naren}@cs.vt.edu, bijaya-adhikari@uiowa.edu

Abstract

Forecasting influenza in a timely manner aids health organizations and policymakers in adequate preparation and decision making. However, effective influenza forecasting still remains a challenge despite increasing research interest. It is even more challenging amidst the COVID pandemic, when the influenza-like illness (ILI) counts is affected by various factors such as symptomatic similarities with COVID-19 and shift in healthcare seeking patterns of the general population. We term the ILI values observed when it is potentially affected as COVID-ILI. Under the current pandemic, historical influenza models carry valuable expertise about the disease dynamics but face difficulties adapting. Therefore, we propose CALI-NET, a neural transfer learning architecture which allows us to ‘steer’ a historical disease forecasting model to new scenarios where flu and COVID co-exist. Our framework enables this adaptation by automatically learning when it should emphasize learning from COVID-related signals and when from the historical model. In such way, we exploit representations learned from historical ILI data as well as the limited COVID-related signals. Our experiments demonstrate that our approach is successful in adapting a historical forecasting model to the current pandemic. In addition, we show that success in our primary goal, adaptation, does not sacrifice overall performance as compared with state-of-the-art influenza forecasting approaches.

1 Introduction

Influenza is a seasonal virus which affects 9–45 million people annually in the United States alone resulting in between 12,000–61,000 deaths. Although the seasonal incidence period of influenza is somewhat consistent annually, the disease progression and severity of a particular seasonal strain are all affected by many social, biological and demographic factors, none of which are completely known.

Forecasting flu outbreak progression each year is an important and non-trivial task. Specifically, accurate forecasts of the start of the flu season, the seasonal peak and increases in rate of incidence can all aid significantly toward informing personalized policy roll out to minimize the effects of a particular flu season. To this end, the Centers for Disease

Control and Prevention (CDC) has been organizing several forecasting tasks, e.g., the FluSight challenge for the past several years, where the goal is to predict weighted influenza-like-illness counts (wILI) throughout the flu season in the United States (Biggerstaff et al. 2016). wILI measures the percentage of healthcare seekers who show influenza like symptoms. Estimating various measures related to the progression of a flu season (such as future incidence over the next few weeks) gives policymakers valuable lead time to plan interventions and optimize supply chain decisions.

In addition to the flu, the world is also experiencing the devastating impacts of the currently unfolding COVID-19 pandemic which has sharply illustrated our enormous vulnerability to emerging infectious diseases. As mentioned previously, the disease progression of flu during each season is already affected by various biological and demographic factors, but now, in part due to symptomatic similarities with COVID and healthcare seeking patterns, wILI counts may get further ‘contaminated’ in the current (and possibly future) influenza seasons. Such miscounting manifests as significant changes in wILI seasonal progression as observed in Fig. 1(a). Here, the wILI curve for the current season 2019-2020 (contaminated by COVID, bold black) clearly shows a very different pattern compared to the previous seasons (in grey). Note that the current season is trimodal, whereas past seasons typically have only one peak value. It is thus imperative that we explicitly model and account for such effects for effective wILI forecasting in the current and future seasons in the presence of a contaminant.

There has been a recent spate of work on flu forecasting using statistical approaches usually trained on historical wILI data (Adhikari et al. 2019). However, this new forecasting problem of adapting to a new emerging pandemic scenario is complex and cannot be addressed by traditional historical wILI methods alone. See Fig. 1(b); current methods based on historical wILI cannot predict the uptrend, while our method (in red) can. The atypical nature of our ‘COVID-ILI’ season may be caused by multiple co-occurring phenomena, e.g., the actual COVID-19 infections, the corresponding shutdowns and societal lock-downs and also changes in the healthcare-seeking behaviors of the public. Due to all these factors, attempting to model COVID-ILI is a challenging problem.

[§]equal contribution

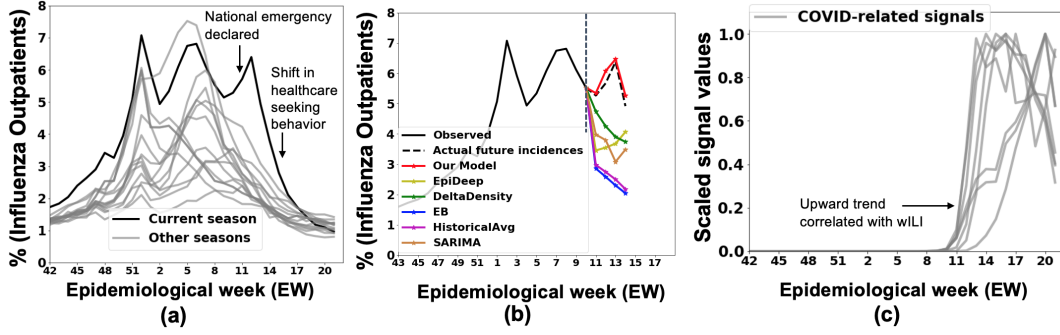


Figure 1: (a) A novel forecasting scenario due to an emerging pandemic. Note the difference between the current and past seasons. (b) Established influenza forecasting methods are not able to adapt to uptrend caused by COVID. (c) Exogenous COVID related signals correlate better with wILI trend changes (due to contamination), which we exploit for more accurate forecasting.

The first challenge here is to capture the atypical trends starting in winter/spring that occur as a result of COVID-19 contamination of wILI. As this feature is exclusive to the current introduction of the pandemic into the ILI season, using only the historical wILI seasons is not sufficient. Hence we propose to leverage external COVID-related signals such as confirmed cases, hospitalizations, and emergency room visits as well. This leads us to the second challenge, viz. how to effectively model the COVID-ILI curve with new COVID-related signals, while also leveraging past prior knowledge present in the previous wILI seasons. However, note that these external signals are not available for historical wILI seasons. How do we address the imbalance in data to leverage both of these data sources? Further, as the contaminated COVID-ILI is a very new phenomenon which suddenly emerged, there is limited data regarding the same from external signals and hence, a significant challenge is also to learn to model it effectively under data paucity.

To address these challenges, we propose CALI-NET (COVID Augmented ILI deep Network), a principled way to 'steer' flu-forecasting models to adapt to new scenarios where flu and COVID co-exist. We employ transfer learning and knowledge distillation approaches to ensure effective transfer of knowledge of the historical wILI trends. We incorporate multiple COVID-related data signals all of which help capture the complex data contamination process showcased by COVID-ILI. As shown in Fig. 1(c), these exogenous signals correlate better with the anomalous trends caused by COVID. Finally, in order to alleviate the data paucity issue, we train a single global architecture with explicit spatial constraints to model COVID-ILI trends of all regions as opposed to previous approaches which have modeled each region separately leading to a superior forecasting performance (See Sec. 5).

Our contributions are as follows:

1. We develop CALI-NET, a novel heterogeneous transfer learning framework to adapt a flu forecasting historical model into the new scenario of COVID-ILI forecasting.
2. We embed CALI-NET with a recurrent neural network including domain-informed spatial constraints to capture the spatiotemporal dynamics across different wILI regions.
3. We also employ a Knowledge Distillation scheme to explic-

itly transfer historical wILI knowledge to our target model in CALI-NET, thereby alleviating the effect of paucity of COVID-ILI data.

4. Finally, we show how CALI-NET succeeds in adaptation, and also perform a rigorous performance comparison of CALI-NET with several state-of-the-art wILI forecasting baselines. In addition, we perform several quantitative and qualitative experiments to understand the effects of various components of CALI-NET.

Overall, more broadly, our work is geared towards adapting a historical model to an emerging disease scenario, and we specifically demonstrate the effectiveness of our approach in the context of wILI forecasting in the COVID-19 emerging disease scenario.

2 Related Work

To summarize, we are the first to address the problem of adapting to shifting trends using transfer learning and knowledge distillation in an epidemic forecasting setting, leveraging exogenous signals as well as historical models. Our research draws from multiple lines of work.

Epidemic Forecasting: Several approaches for epidemic forecasting have been proposed including statistical (Tizzoni et al. 2012; Adhikari et al. 2019; Osthus et al. 2019; Brooks et al. 2018), mechanistic (Shaman and Karspeck 2012; Zhang et al. 2017), and ensemble (Reich et al. 2019a) approaches. Several approaches rely on external signals such as environmental conditions and weather reports (Shaman, Goldstein, and Lipsitch 2010; Tamerius et al. 2013; Volkova et al. 2017), social media (Chen et al. 2016; Lee, Agrawal, and Choudhary 2013), search engine data (Ginsberg et al. 2009; Yuan et al. 2013), and a combination of multiple sources (Chakraborty et al. 2014). Recently, there has been increasing interest in deep learning for epidemic forecasting (Adhikari et al. 2019; Wang, Chen, and Marathe 2019). These methods typically exploit intra and inter seasonal trends. Other approaches like (Venna et al. 2017) are limited to specific situations, e.g., for military populations. However, to the best of our knowledge, there has been no work on developing deep architectures for adapting to trend shifts using exogenous data.

Time Series Analysis: There are several data driven, statistical and model-based approaches that have been developed for time series forecasting such as auto-regression, Kalman filters and groups/panels (Box et al. 2015; Sapankevych and Sankar 2009). Recently, deep recurrent architectures (Hochreiter and Schmidhuber 1997) have shown great promise in learning good representations of temporal evolution (Fu, Zhang, and Li 2016; Muralidhar, Muthiah, and Ramakrishnan 2019; Connor, Martin, and Atlas 1994).

Transfer Learning within heterogeneous domains: This challenging setting of transfer learning with heterogeneous domains (different feature spaces) aims to leverage knowledge extracted from a *source* domain to a different but related *target* domain. (Moon and Carbonell 2017) proposed to learn feature mappings in a common-subspace, and then apply shared neural layers where the transfer would occur. (Li et al. 2019) proposed transfer learning via deep matrix completion. (Yan et al. 2018) formulated this problem as an optimal transport problem using the entropic Gromov-Wasserstein discrepancy. We adapt the method in (Moon and Carbonell 2017) (proposed for a classification task) to our regression setting, for effectively transferring knowledge from the source to the target model in our COVID-ILI forecasting task. Knowledge Distillation (KD) is also a popular transfer learning method, to develop shallow neural networks capable of yielding performance similar to deeper models by learning to "mimic" their behavior (Ba and Caruana 2014; Hinton, Vinyals, and Dean 2015). (Saputra et al. 2019) inspects KD for deep pose regression. The authors propose two regression specific losses, namely the hint loss and the imitation loss which we adapt in this work for COVID-ILI forecasting. Unlike our paper, most KD work has been applied to classification and efforts for adapting KD for regression have been sparse (Saputra et al. 2019; Takamoto, Morishita, and Imaoka 2020).

3 Background

COVID-ILI forecasting task: Here we consider a short term forecasting task of predicting the next k wILI incidence given the data till week $t - 1$ for each US HHS region and the national region. This corresponds to predicting the wILI values for week $\{t, t + 1, \dots, t + k\}$ at week t (matching the exact real-time setting of the CDC tasks) for each region.

We are given a set of historical annual wILI time-series, $Y_i = \{y_i^1, y_i^2, \dots, y_i^t\}$ for each region i . The wILI values have been contaminated by COVID-19 for all weeks $t \geq w$. We also have various exogenous COVID19-related data features $X_i = \{x_i^w, x_i^{w+1}, \dots, x_i^c\}$ for weeks $t \geq w$, where each feature vector \mathbf{d}^i is constructed using various signals such as COVID line list data, test availability, crowd-sourced symptomatic data, and social media. Our task is to forecast the next k wILI incidence for weeks $t \geq w$ for all regions $i \in \mathcal{I}$. Specifically, our novel problem is:

Problem 1 *COVID-ILI Forecasting Problem*

Given: a set of historical annual wILI time-series $Y_i = \{y_i^1, y_i^2, \dots, y_i^t\}$ till week t and the set of COVID-19 related feature vectors $X_i = \{x_i^w, x_i^{w+1}, \dots, x_i^c\}$ for weeks $t \geq w$ for the current season and regions $i \in \mathcal{I}$

Predict: next k wILI incidences $\forall_{i=t+1}^{t+k} y^w$ for all week $t \geq w$ for each region $i \in \mathcal{I}$

Epiddeep for wILI forecasting. EPIDEEP (Adhikari et al. 2019) is a deep neural architecture designed specifically for wILI forecasting. The core idea behind EPIDEEP is to leverage the seasonal similarity between the current season and historical seasons to forecast various metrics of interest such as next incidence values, onset of current season, the seasonal peak value and peak time. To infer the seasonal similarity between current and the historical season, it employs a deep clustering module which learns latent low dimensional embeddings of the seasons.

4 Our Approach

In this section, we describe our method CALI-NET, which models COVID-ILI by incorporating historical wILI knowledge as well as the limited new COVID-related exogenous signals. Next we give an overview of how our approach uses heterogeneous transfer learning (HTL), overcomes data paucity issues, and controls the transfer of only useful knowledge and avoids negative transfer.

4.1 Exploiting Learned Representations from Historical wILI via HTL

We leverage recent advances in HTL to incorporate the rich historical wILI data. To that end, we use the EPIDEEP model as our base model. EPIDEEP was designed to learn representations from historical wILI that embed seasonal and temporal patterns. Here, we adapt the CTHL framework (Moon and Carbonell 2017) to transfer knowledge from EPIDEEP.

In our HTL setting, a modified version of the EPIDEEP model is the source model and we design a feature module (discussed in Sec. 4.2) to be the target model. As depicted in Fig. 2, the embeddings of the source and target are each transformed by modules \mathbf{s} and \mathbf{t} respectively, such that the latent embeddings of the source and target model are placed into a common feature space. In this way, we are projecting knowledge extracted from both heterogeneous feature spaces into a shared latent space. Formally, the transformations may be expressed as $\mathbf{s} : \mathbb{R}^{M_S} \rightarrow \mathbb{R}^{M_J}$ and $\mathbf{t} : \mathbb{R}^{M_T} \rightarrow \mathbb{R}^{M_J}$, where M_S and M_T are the dimensions of the source and target embeddings, respectively, and M_J is the dimension of the joint latent feature space. After projecting representations from the source and the target models into a joint latent feature space, a sequence of shared transformations $\mathbf{f}_1 : \mathbb{R}^{M_J} \rightarrow \mathbb{R}^{M_A}$ and $\mathbf{f}_2 : \mathbb{R}^{M_J} \rightarrow \mathbb{R}$ is applied on them, thereby transporting them both into the same latent space. On top of this architecture, we employ a denoising autoencoder to reconstruct the input data as we find it improves our latent representations. These modules are depicted as \mathbf{s}' and \mathbf{t}' .

4.2 COVID-Augmented Exogenous Model (CAEM)

Our target model from Sec. 4.1 could be a simple feedforward network. Instead, to alleviate the data paucity that exists for the COVID-related exogenous data, we develop the COVID-Augmented Exogenous Model (CAEM) which *jointly* models all regions exploiting regional interplay characteristics. Such

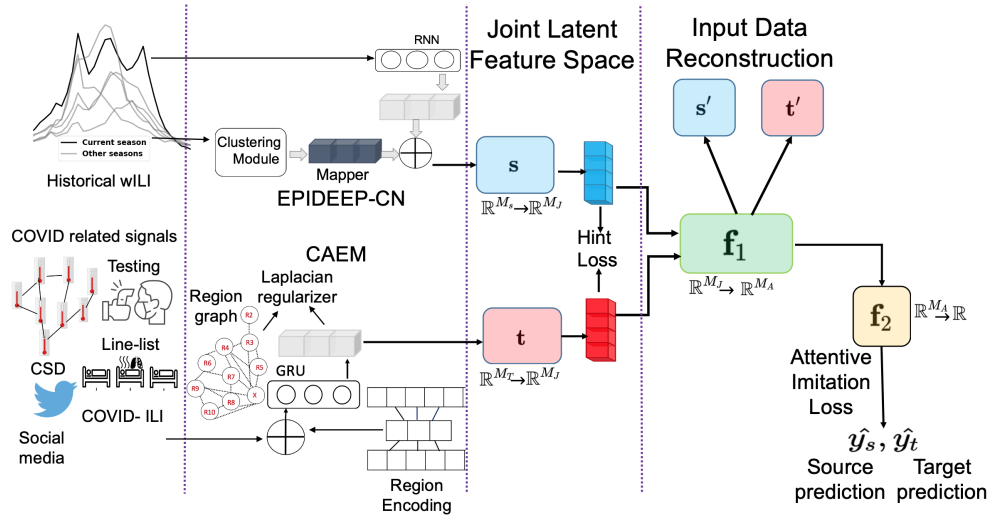


Figure 2: Our proposed model CALI-NET. Our heterogeneous transfer learning architecture is designed to transfer knowledge from EPIDEEP-CN about historical wILI trends to the CAEM module (using exogenous signals) for COVID-ILI forecasting while addressing the challenges of negative transfer, spatial consistency and data paucity.

an approach allows us to extract the most out of our limited training data, while enabling us to employ more sophisticated recurrent architectures to model the sequential nature of the data.

To enable model awareness of multiple regional patterns, we explicitly encode each *region embedding* $\mathbf{r} \in \mathbb{R}^{1 \times h_r}$, passed to CAEM along with the exogenous input data of the region for a particular week. The region embedding is obtained from embeddings produced by an autoencoder whose task is to reconstruct one-hot encodings of each region.

The data we consider exhibit sequential dependencies. In order to model these dependencies, we employ the popular GRU recurrent neural architecture (Cho et al. 2014). The GRU is trained to encode temporal dependencies using data from week $t - W$ to week $t - 1$ and predict values for week $t + k$. At each step of recurrence, the GRU receives as input, exogenous data signals $\mathbf{x}_i^{t-w} \in \mathbb{R}^{1 \times l}$ (for week $t - w$ and region i) and the region embedding r_i , both concatenated to form the full GRU input. For simplicity, henceforth, we consider $\mathbf{x}_i^{t-w} \in \mathbb{R}^{1 \times l + h_r}$ to represent this concatenated input to the GRU (l is the number of different data signals we employ and h_r is the dimension of the latent region embedding obtained from the CAEM Region Embedding autoencoder).

Laplacian Regularization: Infectious diseases like COVID and flu naturally also show strong spatial correlations and to capture this aspect of the wILI season evolution across different regions effectively, we incorporate spatial constraints using Laplacian Regularization (Belkin, Matveeva, and Niyogi 2004) and predict COVID-ILI values for all regions jointly. Let us consider the region graph $G(V, E)$ where V (vertices) indicates the number of regions (11 in our case including the national region) and E indicates edges between the vertices. Two regions are considered to have an edge between them if they are bordering each other. We construct G based on region demarcations provided by the HHS/CDC and connect

the national region to all other regions.

The optimization objective for CAEM is as follows:

$$\min_{\Theta_{RE}\Theta_F} \|F(\mathbf{X}^{t-W:t-1}; \Theta_F) - Y^t\|_2^2 + RE(\mathbf{E}; \Theta_{RE}) + Tr(\mathbf{h}^T \mathbf{L} \mathbf{h}^2) \quad (1)$$

In Eq. 1, Θ_{Re} , Θ_F represent the model parameters associated with the *region embedding* (RE) function and the recurrent *forecasting* (F) function respectively. The input to the recurrent forecasting model (F), $\mathbf{X}^{t-W:t-1} \in \mathbb{R}^{|V| \times l + h_r}$ is the historical COVID-related exogenous data for the past W weeks for all 11 regions (along with the regional embedding for each) which is appropriately handled within the GRU. The output of F, $Y^t \in \mathbb{R}^{|V| \times 1}$ for week t includes forecasts for all 11 regions. The region embedding is generated using an autoencoder which accepts the one-hot encoding for all regions $\mathbf{E} \in \mathbb{B}^{|V| \times |V|}$. Finally, $\mathbf{h} \in \mathbb{R}^{1 \times h_r}$ is the hidden representation of the input sequence generated by the forecasting model F at the end of the recurrence which is used to enforce regional representation similarity governed by the normalized Laplacian (\mathbf{L}) of graph G . Laplacian regularization has been shown to systematically enforce regional similarity, effectively capturing spatial correlations (Subbian and Banerjee 2013). Both the RE and F tasks of CAEM are jointly trained coupled with Laplacian regularization. It must be noted that when integrated into CALI-NET, the function F includes the GRU and the transformations $\mathbf{t}, \mathbf{f}_1, \mathbf{f}_2$ to yield the final k -week ahead predictions.

4.3 Attentive Knowledge Distillation Loss

A mechanism for the target model to exercise control over knowledge transfer and prevent negative transfer is necessary in our setting to avoid the transfer of possibly erroneous predictions made by EPIDEEP for the atypical portions of the current influenza season. To enable this, we employ attentive

knowledge distillation (KD) techniques. Recently, (Saputra et al. 2019) has employed KD in deep pose estimation. We noticed our modification of this method is capable of not only transferring knowledge from EPIDEEP (our source model) to CAEM (our target model) but also showcase how to selectively transfer knowledge based on the quality of source model predictions.

Adapting EPIDEEP: In order to achieve effective transfer of knowledge from EPIDEEP to CAEM, we modify the existing EPIDEEP architecture. EPIDEEP, by design, requires a different model to be trained for each week in the season which is not ideal for effective knowledge transfer. Hence, to prevent this, we modify EPIDEEP into EPIDEEP-CN (EpiDeep-CALI-NET) which incrementally re-trains the same model for each week in the season, thereby allowing the KD losses to be applied to the same set of EPIDEEP-CN parameters, enabling more efficient knowledge transfer to CAEM. Specifics about EPIDEEP-CN are in our appendix.

The training datasets for EPIDEEP-CN and CAEM are not the same, however they share an overlapping subset of data, from January 2020 onward when the COVID pandemic started. Therefore, we enforce the *KD loss* only on this subset of the training data. Our KD loss is composed of two terms: imitation loss \mathcal{L}_{Im} and hint loss $\mathcal{L}_{\text{Hint}}$, described mathematically as follows,

$$\mathcal{L}_{KD} = \alpha \frac{1}{n} \sum_{i=1}^n \Phi_i \underbrace{\|\hat{y}_s - \hat{y}_t\|_i^2}_{\mathcal{L}_{\text{Im}}} + \Phi_i \underbrace{\|\Psi_s - \Psi_t\|_i^2}_{\mathcal{L}_{\text{Hint}}} \quad (2)$$

where $\Phi_i = \left(1 - \frac{\|\hat{y}_s - y\|_i^2}{\eta}\right)$, and Ψ_s and Ψ_t are the output embeddings of \mathbf{s} and \mathbf{t} , respectively; $i \in \{1, \dots, n\}$ is the index for each training observation, and n the batch size; $\eta = \max(e_s) - \min(e_s)$ is a normalizing factor (i.e range of squared error losses of source model) and $e_s = \{\|y - \hat{y}_s\|_j^2 : j = 1, \dots, N\}$, the actual set of squared errors between the source predictions and ground truth. N is the total number of observations in the overlap training data; Φ_i is the attention weight that is given to a training observation. The attention is a function of how well the source model is able to predict (\hat{y}_s) a particular ground truth target y . The attention weights are applied over the imitation loss between the source predictions (\hat{y}_s) and the ground truth (\hat{y}_t) as well as over the hint loss between the latent output embeddings Ψ_s and Ψ_t to ensure transfer of knowledge at multiple levels in the architecture from the source EPIDEEP-CN to the target CAEM. The goal of KD is to enforce a unidirectional transfer from the source (EPIDEEP-CN) to the target (CAEM) model. Hence KD losses do not affect the representations learned by EPIDEEP-CN and module \mathbf{s} .

5 Experiments

Setup. All experiments are conducted using a 4 Xeon E7-4850 CPU with 512GB of 1066 Mhz main memory. Our method is very fast, training for one predictive task in about 3 mins. Here, we present our results for next incidence prediction (i.e. $k = 1$). We present results for next-two incidence prediction in the appendix, which are similar. Note that we

define T_1 as the period of non-seasonal rise of wILI due to contamination by COVID-19 related issues (EWs 9-11), T_2 as the time period when COVID-ILI trend is declining more in tune with the wILI pattern (EWs 12-15), and T as the entire course (EWs 9-15).

Data. We use the historical weighted Influenza-like Illness (wILI) data released by the CDC which collects it through the Outpatient Influenza-like Illness Surveillance Network (ILINet). ILINet consists of more than 3,500 outpatient healthcare providers all over the US. We refer to wILI from June 2004 until Dec 2019 as **historical wILI**, and wILI from January 2020 as **COVID-wILI**. Next, Table 1 details the various signal types we employ for COVID-related exogenous data. A more detailed description of each data signal can be found in the appendix. All datasets are publicly available and were collected in May 2020.

Goals. In our experiments we aim to demonstrate that our method CALI-NET can systematically steer a historical model to the new COVID-ILI scenario by enabling it to learn from Covid-related signals, when appropriate. We are interested in determining whether our model can transfer useful information from the historical model (i.e. EPIDEEP) when required and if it can prevent transfer of detrimental information. Specifically, our questions are:

Transfer Learning

Q1. Is CALI-NET able to achieve successful positive transfer to model the contamination of wILI values?

Q2. Does CALI-NET prevent negative transfer by automatically recognizing when wILI and COVID-19 trends deviate?

Forecasting Performance

Q3. Does CALI-NET’s emphasis on transfer learning sacrifice overall performance with respect to state-of-the-art methods?

Ablation Studies

Q4. How does each facet of CALI-NET affect COVID-ILI forecasting performance?

Q5. What data signals are most relevant to COVID-ILI forecasting?

Q1 and Q2, which are about transfer learning, are aligned with the main goal of this paper. In Q3, we are interested in determining whether CALI-NET sacrifices any overall forecasting performance, as compared to the state-of-the-art (SOTA) baselines, by being too focused on balancing the transfer of knowledge? In Q4 and Q5 we analyze importance of different components and data signals to performance.

Training and Optimization. For training CALI-NET, we do the following. We found that, for practical purposes, it is convenient to pre-train EPIDEEP-CN, and then remove its last feedforward layers (decoder). Hence the concatenated output of the RNN encoder and the embedding mapper are input to module \mathbf{s} . During joint training, we do not modify EPIDEEP-CN’s pre-trained parameters. As recommended in (Moon and Carbonell 2017), we train the HTL architecture in an alternating fashion.

Baselines. We use traditional historical wILI forecasting methods used in literature (Reich et al. 2019a): EPIDEEP, extended DELTA DENSITY from Delphi Group (Brooks et al. 2018) (which is SOTA as the top performing method in recent CDC influenza forecasting challenges (Reich et al. 2019b)), SARIMA from ReichLab (Ray et al. 2017) (sea-

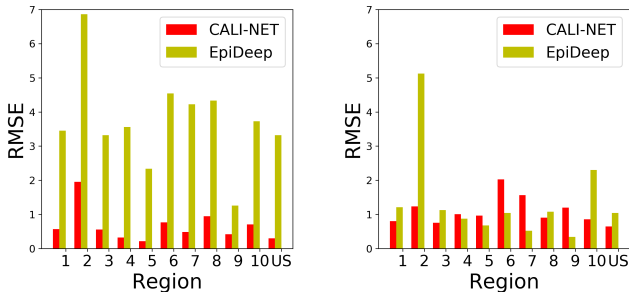
Table 1: Overview of COVID-Related Exogenous Data.

| Type of signal | Description | Signals | Source |
|-----------------------------------|--|--|--------------------------------|
| (DS1) Line list based | They are a direct function of the disease spread | 1. Confirmed cases; 2. UCI beds; 3. Hospitalizations; 4. People on ventilation; 5. Recovered; 6. Deaths; 7. Hospitalization rate; 8. ILI ER visits; 9. CLI ER visits | (cov 2020; cdc 2020; jhu 2020) |
| (DS2) Testing based | Related to social policy and behavioral considerations | 10. People tested; 11. Negative cases; 12. Emergency facilities reporting; 13. No. of providers; | (cov 2020; cdc 2020) |
| (DS3) Crowdsourced symptoms based | Crowdsourced symptomatic data from personal devices | 14. Digital thermometer readings; | (Miller et al. 2018) |
| (DS4) Social media | Social media activity | 15. Health Related Tweets | (Dredze et al. 2014) |

sonal autoregressive method, top performing in recent CDC challenges), and EMPIRICAL BAYES (Brooks et al. 2015) (which leverages transformation of historical seasons to forecast the current season), and HIST (commonly used baseline which makes forecast based on weekly average of the historical seasons).

5.1 Q1: Leveraging positive transfer for Covid-contaminated wILI

The effect of contamination is the most pronounced in T_1 , leading to the COVID-ILI curve exhibiting uncharacteristic non-trivial progression dynamics. Therefore, to effectively steer our historical model, CALI-NET automatically leverages positive transfer of Covid-related signals into EPIDEEP. The effect of this automatic positive transfer is shown in Fig. 3(a) where we see that CALI-NET significantly outperforms EPIDEEP across *all regions*, thanks to our architecture.



(a) Positive transfer stage (b) Negative transfer stage

Figure 3: (a) Our CALI-NET framework effectively achieves good forecasts of the uncharacteristic trend in period T_1 by steering our influenza forecasting historical model EPI-DEEP with knowledge learned from Covid-related signals. (b) Shows forecasting errors from period T_2 , when the COVID-ILI trend is declining more in tune with the traditional wILI pattern. We notice that CALI-NET is competitive with EPI-DEEP, also outperforming it in 6 out of 11 regions while remaining competitive in the rest of the regions.

5.2 Q2: Does CALI-NET prevent negative transfer automatically?

Having showcased the adaptation of CALI-NET in T_1 , we now show in Fig. 3(b) that our method is effective at preventing negative transfer when wILI is no longer aligned with the exogenous COVID signals (i.e., period T_2). In the first place, in some regions the wILI trajectory were never significantly affected by COVID as confirmed COVID cases started to increase significantly only once the influenza season ended. Second, COVID-affected wILI trajectories of regions displayed a subsequent downtrend after a few weeks. This may be due to the change in care-seeking behavior of outpatients (Kou et al. 2020). In this stage, preventing negative transfer from COVID-related signals is needed, such that our model displays more characteristics of traditional influenza models. From Fig. 3(b), we see that CALI-NET is better than EPI-DEEP in a majority of the regions indicating that it is able to effectively stop knowledge from misaligned COVID signals from adversely affecting forecasting accuracy thereby effectively preventing negative transfer.

5.3 Q3: Does CALI-NET sacrifice overall performance?

Sec 5.2 and 5.3 show that CALI-NET successfully achieves the main goal of the paper i.e. steering a historical model in a novel scenario. We now study if we sacrifice any performance in this process. To this end, we compare CALI-NET with the traditional SOTA wILI forecasting approaches for the entire course T . Specifically, we quantify the number of regions (among all 11), where each method outperforms all others. Fig. 4 showcases our findings. Overall, CALI-NET is able to match the performance of the SOTA historical wILI forecasting models in forecasts for the entire course T and is the top performer in 5 of 11 regions and is one of top 2 best models in 10 out of 11 regions. Note that the traditional wILI baselines do not capture the non-seasonal rise of wILI due to COVID contamination in T_1 (see Figure 1 and the appendix). Hence, we note that CALI-NET is the best-suited approach for real-time forecasting in a novel scenario as it captures the non-seasonal patterns while maintaining overall performance. Moreover, we also noticed that CALI-NET outperforms all baselines in regions worst affected by COVID (see appendix).

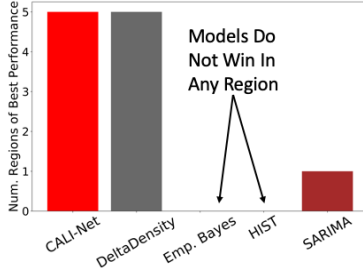
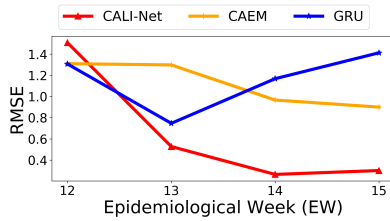


Figure 4: Overall results of CALI-NET compared to Empirical Bayes and SOTA baseline DeltaDensity. We show number of regions in which each model yields best performance and notice CALI-NET outperforms other models in 5 out of 11 regions, on par with DeltaDensity which also yields best performance in 5 other regions with SARIMA being the best in a single region (i.e., Region 9). Models performing within 1% of best model per region are considered equivalent best performers. Hence CALI-NET yields competitive performance across the entire course T .

5.4 Q4 and Q5: Module, Data and Parameter Importance and Sensitivity

Justification for CAEM architecture. We conducted an ablation study testing the three components of CAEM: (a) regional reconstruction, (b) Laplacian regularization, and (c) the recurrent model. We found that removing each of them degrades performance showing their individual effectiveness.

Module Performance Analysis. The figure below showcases RMSE evolution over period T_2 for the national region for CALI-NET and sub-models of CALI-NET that do not have transfer learning capability. Both GRU (standard gated recurrent unit model) and the standalone CAEM model use exogenous data as CALI-NET does. CALI-NET is the only model able to adapt quickly to the downtrend in period T_2 , due to the effect of the HTL framework which prevents negative transfer of knowledge from COVID related signals, while other models fail to adapt and in fact predict rising or flat wILI forecasts.



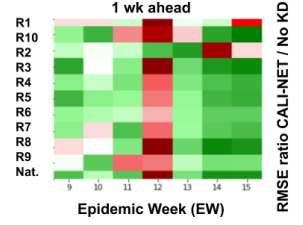
From Sec. 5.1 - 5.3, we see that CALI-NET is the *only* method capable of capturing both the initial uptrend of COVID-ILI and the subsequent decline effectively, showing its usefulness for emerging diseases.

Effect of KD. We perform an ablation study to understand the contribution of the proposed KD losses. Often the usefulness of source (EPIDEEP-CN) and target (CAEM) modules vary depending on the usefulness of the historical and exogenous data sources. Our attentive KD distillation losses provide structure and balance to the transferred knowledge.

We compare 1-week ahead forecast-

ing performance of CALI-NET and a variant of CALI-NET with KD losses removed.

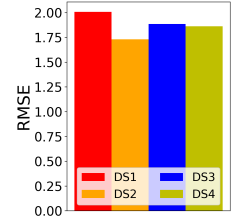
Specifically, see Fig. right; each box is colored by the ratio of RMSE of CALI-NET and its variant (capped at -1 and 1 to help visualization). Green cells indicate that CALI-NET does better while red cells indicate that CALI-NET w/o KD losses does better.



We see that for 1-week ahead forecasting, structuring the knowledge transferred from EPIDEEP proves to be valuable for most EWs. However, for long-term forecasting, KD losses seem to downgrade guidance of EPIDEEP-CN (results in appendix). This may be because, the season seems to revert to typical behavior in the time-frame predicted in long-term forecasts.

Contribution of exogenous signals. In the figure below, we can see the average overall RMSE obtained when a single data bucket was removed during the training of CALI-NET.

We noticed that line list based data (DS1) is very helpful in COVID-ILI forecasting while the effectiveness of testing (DS2) and crowdsourced based (DS3) data is slightly more varied across regions, an observation that resolves Q5. This also suggests that data closer to the disease is more reliable. More detailed results (regional breakdown) are in the appendix.



Parameter Sensitivity. For the hyperparameters of CALI-NET, we perform thorough experiments and demonstrate the robustness of our method. Details in the appendix.

6 Discussion

Here we introduced the challenging COVID-ILI forecasting task, and proposed our novel approach CALI-NET. We show the usefulness of a principled method to transfer relevant knowledge from an existing deep flu forecasting model (based on rich historical data) to one relying on relevant but limited recent COVID-related exogenous signals. Our method is based on carefully designed components to avoid negative transfer (by attentive KD losses), promote spatial consistency (via Laplacian losses in a novel recurrent architecture CAEM), and also handle data paucity (via the global nature of CAEM and other aspects). CALI-NET effectively captures non-trivial atypical trends in COVID-ILI evolution whereas other models and baselines do not. We also demonstrate how each of our components and data signals is important and useful for performance. These results provide guidance for steering forecasting models in an emerging disease scenario. In future, we believe our techniques can be applied to other source models (in addition to EPIDEEP-CN), as well as designing more sophisticated architectures for the target CAEM model. We can also explore adding interpretability to our forecasts for additional insights.

Ethical and Broader Impact

This work has the strong potential of impacting local and national policies on interventions such as stay-at-home orders and vaccine deployments especially in Fall when the flu season will coincide with newer waves of COVID. The proposed approach should also be more broadly useful for other infectious diseases where we need to steer historical models in novel emerging scenarios. The datasets we use in this paper are publicly available. The line-lists we use consist of anonymous COVID-19 patients with limited meta information on location (at ZIP code level), age, gender, and time of infection. As such, we are not leveraging any sensitive patient information. The predictions may be affected by any systematic biases in data collection (for example, some regions might have poorer surveillance and reporting capabilities). There is limited potential for misuse of our algorithms and/or data sources as we do not employ any identifying information but our analysis can shed insight into inequities that exist in disease incidence across regions and across communities.

Acknowledgments

This paper is based on work supported by the NSF (Expeditions CCF-1918770, CAREER IIS-1750407, RAPID IIS-2027862, Medium IIS-1955883, NRT DGE-1545362, IIS-1633363), CDC MInD-Healthcare U01CK000531-Supplement, funds from Georgia Tech Research Institute (GTRI) and funds/computing resources from Georgia Tech.

References

- Adhikari, B.; Xu, X.; Ramakrishnan, N.; and Prakash, B. A. 2019. Epiddeep: Exploiting embeddings for epidemic forecasting. In *Proceedings of the 25th ACM SIGKDD International Conference on Knowledge Discovery & Data Mining*, 577–586.
- Ba, J., and Caruana, R. 2014. Do deep nets really need to be deep? In *Advances in neural information processing systems*, 2654–2662.
- Belkin, M.; Matveeva, I.; and Niyogi, P. 2004. Regularization and semi-supervised learning on large graphs. In *International Conference on Computational Learning Theory*, 624–638. Springer.
- Biggerstaff, M.; Alper, D.; Dredze, M.; Fox, S.; Fung, I. C.-H.; Hickmann, K. S.; Lewis, B.; Rosenfeld, R.; Shaman, J.; Tsou, M.-H.; et al. 2016. Results from the centers for disease control and prevention’s predict the 2013–2014 influenza season challenge. *BMC infectious diseases* 16(1):357.
- Box, G. E.; Jenkins, G. M.; Reinsel, G. C.; and Ljung, G. M. 2015. *Time series analysis: forecasting and control*. John Wiley & Sons.
- Brooks, L. C.; Farrow, D. C.; Hyun, S.; Tibshirani, R. J.; and Rosenfeld, R. 2015. Flexible modeling of epidemics with an empirical bayes framework. *PLoS computational biology* 11(8):e1004382.
- Brooks, L. C.; Farrow, D. C.; Hyun, S.; Tibshirani, R. J.; and Rosenfeld, R. 2018. Nonmechanistic forecasts of seasonal influenza with iterative one-week-ahead distributions. *PLOS Computational Biology* 14(6):e1006134.
2020. Weekly U.S. Influenza Surveillance Report CDC. <https://www.cdc.gov/flu/weekly/index.htm>.
- Chakraborty, P.; Khadivi, P.; Lewis, B.; Mahendiran, A.; Chen, J.; Butler, P.; Nsoesie, E. O.; Mekaru, S. R.; Brownstein, J. S.; Marathe, M. V.; et al. 2014. Forecasting a moving target: Ensemble models for ili case count predictions. In *Proceedings of the 2014 SIAM international conference on data mining*, 262–270. SIAM.
- Chen, L.; Hossain, K. T.; Butler, P.; Ramakrishnan, N.; and Prakash, B. A. 2016. Syndromic surveillance of flu on twitter using weakly supervised temporal topic models. *Data mining and knowledge discovery* 30(3):681–710.
- Cho, K.; Van Merriënboer, B.; Gulcehre, C.; Bahdanau, D.; Bougares, F.; Schwenk, H.; and Bengio, Y. 2014. Learning phrase representations using rnn encoder-decoder for statistical machine translation. *arXiv preprint arXiv:1406.1078*.
- Connor, J. T.; Martin, R. D.; and Atlas, L. E. 1994. Recurrent neural networks and robust time series prediction. *IEEE transactions on neural networks* 5(2):240–254.
2020. The COVID Tracking project. <https://covidtracking.com/>.
- Dredze, M.; Cheng, R.; Paul, M. J.; and Broniatowski, D. 2014. Healthtweets. org: a platform for public health surveillance using twitter. In *Workshops at the Twenty-Eighth AAAI Conference on Artificial Intelligence*.
- Fu, R.; Zhang, Z.; and Li, L. 2016. Using lstm and gru neural network methods for traffic flow prediction. In *2016 31st Youth Academic Annual Conference of Chinese Association of Automation (YAC)*, 324–328. IEEE.
- Ginsberg, J.; Mohebbi, M. H.; Patel, R. S.; Brammer, L.; Smolinski, M. S.; and Brilliant, L. 2009. Detecting influenza epidemics using search engine query data. *Nature* 457(7232):1012.
- Hinton, G.; Vinyals, O.; and Dean, J. 2015. Distilling the knowledge in a neural network. *arXiv preprint arXiv:1503.02531*.
- Hochreiter, S., and Schmidhuber, J. 1997. Long short-term memory. *Neural computation* 9(8):1735–1780.
2020. COVID-19 Map. <https://coronavirus.jhu.edu/map.html>.
- Kou, S.; Yang, S.; Chang, C.-J.; Ho, T.-H.; and Graver, L. 2020. Unmasking the actual covid-19 case count. *Clinical Infectious Diseases*.
- Lee, K.; Agrawal, A.; and Choudhary, A. 2013. Real-time disease surveillance using twitter data: demonstration on flu and cancer. In *Proceedings of the 19th ACM SIGKDD international conference on Knowledge discovery and data mining*, 1474–1477. ACM.
- Li, H.; Pan, S. J.; Wan, R.; and Kot, A. C. 2019. Heterogeneous Transfer Learning via Deep Matrix Completion with Adversarial Kernel Embedding. *Proceedings of the AAAI Conference on Artificial Intelligence* 33:8602–8609.

- Miller, A. C.; Singh, I.; Koehler, E.; and Polgreen, P. M. 2018. A smartphone-driven thermometer application for real-time population-and individual-level influenza surveillance. *Clinical Infectious Diseases* 67(3):388–397.
- Moon, S., and Carbonell, J. G. 2017. Completely Heterogeneous Transfer Learning with Attention-What And What Not To Transfer. In *IJCAI*, volume 1, 1–2. Issue: 1.
- Muralidhar, N.; Muthiah, S.; and Ramakrishnan, N. 2019. Dyat nets: dynamic attention networks for state forecasting in cyber-physical systems. In *Proceedings of the 28th International Joint Conference on Artificial Intelligence*, 3180–3186. AAAI Press.
- Osthus, D.; Gattiker, J.; Friedhorsky, R.; Del Valle, S. Y.; et al. 2019. Dynamic bayesian influenza forecasting in the united states with hierarchical discrepancy (with discussion). *Bayesian Analysis* 14(1):261–312.
- Ray, E. L.; Sakrejda, K.; Lauer, S. A.; Johansson, M. A.; and Reich, N. G. 2017. Infectious disease prediction with kernel conditional density estimation: Infectious disease prediction with kernel conditional density estimation. *Statistics in Medicine* 36(30):4908–4929.
- Reich, N. G.; McGowan, C. J.; Yamana, T. K.; Tushar, A.; Ray, E. L.; Osthus, D.; Kandula, S.; Brooks, L. C.; Crawford-Crudell, W.; Gibson, G. C.; et al. 2019a. Accuracy of real-time multi-model ensemble forecasts for seasonal influenza in the us. *PLoS computational biology* 15(11).
- Reich, N. G.; McGowan, C. J.; Yamana, T. K.; Tushar, A.; Ray, E. L.; Osthus, D.; Kandula, S.; Brooks, L. C.; Crawford-Crudell, W.; Gibson, G. C.; Moore, E.; Silva, R.; Biggerstaff, M.; Johansson, M. A.; Rosenfeld, R.; and Shaman, J. 2019b. A Collaborative Multi-Model Ensemble for Real-Time Influenza Season Forecasting in the U.S. preprint, Epidemiology.
- Sapankevych, N. I., and Sankar, R. 2009. Time series prediction using support vector machines: a survey. *IEEE Computational Intelligence Magazine* 4(2).
- Saputra, M. R. U.; de Gusmao, P. P.; Almalioglu, Y.; Markham, A.; and Trigoni, N. 2019. Distilling knowledge from a deep pose regressor network. In *Proceedings of the IEEE International Conference on Computer Vision*, 263–272.
- Shaman, J., and Karspeck, A. 2012. Forecasting seasonal outbreaks of influenza. *Proceedings of the National Academy of Sciences* 109(50):20425–20430.
- Shaman, J.; Goldstein, E.; and Lipsitch, M. 2010. Absolute humidity and pandemic versus epidemic influenza. *American journal of epidemiology* 173(2):127–135.
- Subbian, K., and Banerjee, A. 2013. Climate multi-model regression using spatial smoothing. In *Proceedings of the 2013 SIAM International Conference on Data Mining*, 324–332. SIAM.
- Takamoto, M.; Morishita, Y.; and Imaoka, H. 2020. An efficient method of training small models for regression problems with knowledge distillation. *arXiv preprint arXiv:2002.12597*.
- Tamerius, J. D.; Shaman, J.; Alonso, W. J.; Bloom-Feshbach, K.; Uejio, C. K.; Comrie, A.; and Viboud, C. 2013. Environmental predictors of seasonal influenza epidemics across temperate and tropical climates. *PLoS pathogens* 9(3):e1003194.
- Tizzoni, M.; Bajardi, P.; Poletto, C.; Ramasco, J. J.; Balcan, D.; Gonçalves, B.; Perra, N.; Colizza, V.; and Vespignani, A. 2012. Real-time numerical forecast of global epidemic spreading: case study of 2009 a/h1n1pdm. *BMC medicine* 10(1):165.
- Venna, S. R.; Tavanaei, A.; Gottumukkala, R. N.; Raghavan, V. V.; Maida, A.; and Nichols, S. 2017. A novel data-driven model for real-time influenza forecasting. *bioRxiv* 185512.
- Volkova, S.; Ayton, E.; Porterfield, K.; and Corley, C. D. 2017. Forecasting influenza-like illness dynamics for military populations using neural networks and social media. *PloS one* 12(12):e0188941.
- Wang, L.; Chen, J.; and Marathe, M. 2019. Defsi: Deep learning based epidemic forecasting with synthetic information. In *Proceedings of the AAAI Conference on Artificial Intelligence*, volume 33, 9607–9612.
- Yan, Y.; Li, W.; Wu, H.; Min, H.; Tan, M.; and Wu, Q. 2018. Semi-Supervised Optimal Transport for Heterogeneous Domain Adaptation. In *Proceedings of the Twenty-Seventh International Joint Conference on Artificial Intelligence*, 2969–2975. Stockholm, Sweden: International Joint Conferences on Artificial Intelligence Organization.
- Yuan, Q.; Nsoesie, E. O.; Lv, B.; Peng, G.; Chunara, R.; and Brownstein, J. S. 2013. Monitoring influenza epidemics in china with search query from baidu. *PloS one* 8(5):e64323.
- Zhang, Q.; Perra, N.; Perrotta, D.; Tizzoni, M.; Paolotti, D.; and Vespignani, A. 2017. Forecasting seasonal influenza fusing digital indicators and a mechanistic disease model. In *Proceedings of the 26th International Conference on World Wide Web*, 311–319. International World Wide Web Conferences Steering Committee.

Appendix

In this appendix, we provide further details about overall CALI-NET performance and about EPIDEEP-CN and the COVID-related exogenous data. In addition, we study how various components of CALI-NET and the COVID-related data signals used, each contribute to the final performance, and also subsequently characterize the sensitivity of CALI-NET to important hyperparameters.

In Sec. A1 we characterize the performance of CALI-NET and SOTA baselines for each US HHS region and the national region. Sec. 5.4 of the main paper, under **Effect of KD**, showcases the important results obtained from employing knowledge distillation (KD) in CALI-NET. We expand on these results in Sec. A2. Due to a lack of space, we were unable to provide full details about the contribution of each COVID-related exogenous data bucket to CALI-NET performance in Sec. 5.4 (**Contribution of exogenous signals**) of the main paper. Hence, we provide further details about the data ablation experiment we conducted characterizing the effect of each COVID-related exogenous data bucket in Sec. A3. We showcase results about parameter sensitivity of the CALI-NET model, and justify our choice of different facets of the CAEM architecture in Sec. A4. Sec. A5 provides details about how EPIDEEP has been adapted for use in CALI-NET, initially mentioned in Sec. 4.3 of the main paper under the subheading **Adapting EpiDeep**. We have briefly mentioned all the COVID-related exogenous data signals in Table 1 (Sec. 5 **Experiments**) of the main paper, Sec. A6 provides further details about each specific COVID-related exogenous signal.

A1: Performance of CALI-NET against state-of-the-art baselines

We extend the analysis performed in Sec. 5.1 of the main paper and further inspect the positive transfer capabilities of CALI-NET during phase T_1 by showcasing a region-wise performance characterization of CALI-NET along with the performance of other SOTA baselines employed in the main paper. We characterize model forecasting performance for both one week ahead and two week ahead contexts. We notice from Fig. 5(a) and (b) that CALI-NET comfortably outperforms all other models in the period T_1 by yielding more accurate forecasts of the initial non-seasonal rise in wILI in a majority of the regions for both one week ahead and two week ahead forecasting cases. We specifically notice that CALI-NET is the best performing wILI forecasting model for the worst COVID-19 affected region (i.e Region 2 which is the region containing New York City) and is also the best at forecasting the national wILI trend in time period T_1 in both the one week ahead and two week ahead cases.

A2: Effects of Knowledge Distillation (KD)

Extending the discussion in Sec. 5.4 of the main paper, we further elucidate the effect of KD losses by providing additional ablation study results not included in the main paper due to lack of space. In our CALI-NET approach, the goal of the KD losses was to systematically leverage useful knowledge from EPIDEEP-CN and CAEM at appropriate times.

In Fig. 6, where, green squares indicate that CALI-NET with KD losses performs better than the variant without KD losses while the red squares indicate the opposite behavior, we notice that in the 1 week and 2 week ahead contexts, the KD losses are helpful in a majority of the cases. In the 2-week ahead case, we notice that the variant of CALI-NET without KD losses performs better for EW 11,12. This is due to the season reverting back to typical behavior. We notice that for weeks 13 - 15, the variant of CALI-NET with KD losses adapts effectively and is the best performing model once again for EW 13 - 15. In both the plots, we also notice that the region worst affected by COVID-19 namely Region 2 (the region containing New York City), is better modeled by CALI-NET with KD losses than by the variant of CALI-NET without KD losses. This showcases the effectiveness of the KD losses in CALI-NET to systematically incorporate the effect of COVID-related exogenous data as well as knowledge from historical models (EPIDEEP-CN) to model wILI.

A3: Contribution of Exogenous Data Signals

In addition to the overall data ablation study conducted in Sec. 5.4 of the main paper, we also characterize region-wise effects of different exogenous signals employed. In Fig. 7, notice that the line-listing data (DS1) is very helpful in COVID-ILI forecasting for all regions while the effectiveness of the crowd-sourced (DS3) and testing data (DS2) is slightly more varied across regions. Finally, we notice that the social media activity data (DS4) which captures COVID-ILI related chatter, is especially helpful in regions 2 and 6.

A4: Justification for CAEM Architecture and Parameter Sensitivity

As outlined in the paper, we employ CAEM as the target model which learns to systematically incorporate knowledge from historical wILI forecasting methods like EPIDEEP-CN (as a function of the HTL architecture with KD proposed in CALI-NET) as well as to incorporate knowledge from COVID-related data signals in modeling the atypical COVID-ILI season. The CAEM model was specifically designed keeping in mind the various underlying properties influencing wILI like region interplay between proximal regions as well as the sequential nature of the data. In order to characterize the effectiveness of the CAEM module, we study the effect of its specific facets in the context of the overall performance CALI-NET yields when the various components of CAEM are removed.

Three major facets of CAEM are the Laplacian regularization to incorporate regional inter-dependencies, the GRU recurrent architecture to incorporate the sequential nature of the underlying COVID-related and wILI signals and finally the regional reconstruction related to the regional embedding denoting the region of a particular input data point. In Table. 2, we characterize the performance of CALI-NET with variants of CAEM, namely:

1. **CALI-NET w/o GRU**: Here, the CAEM module in CALI-NET has a feed-forward network instead of the GRU architecture.

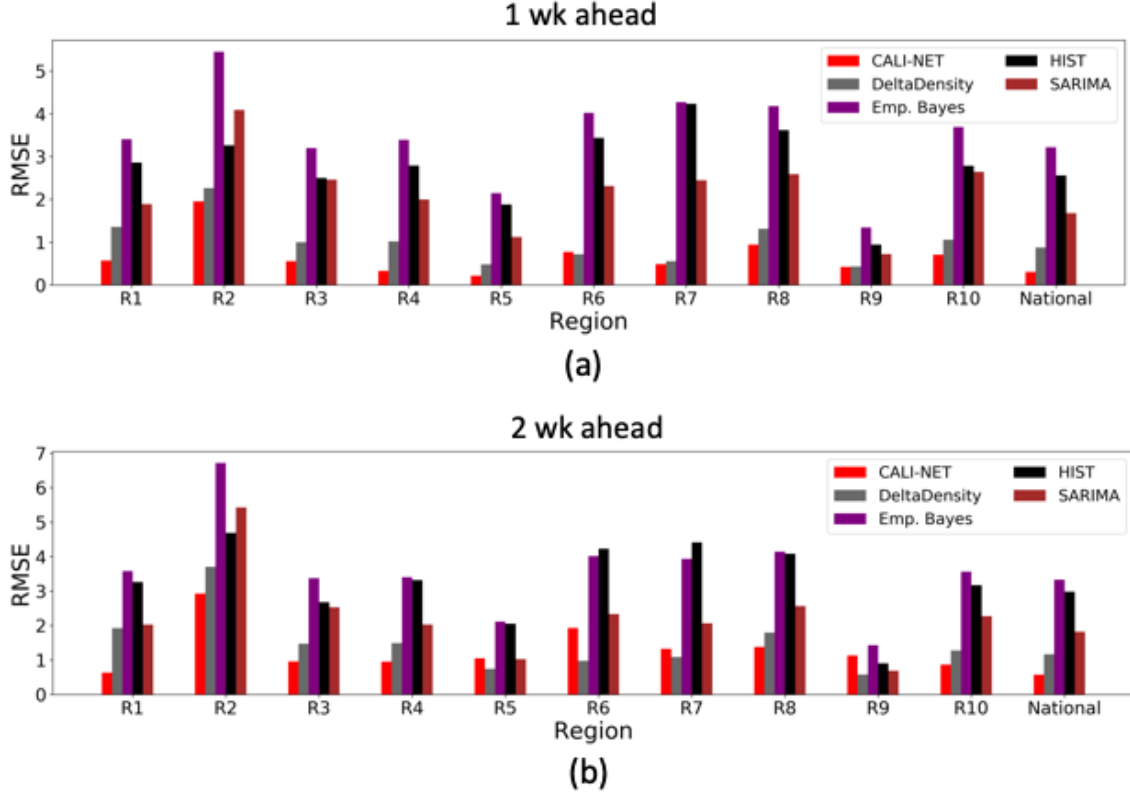


Figure 5: Region-wise breakdown of forecasting error (RMSE) in time period T_1 , to characterize performance of CALI-NET and other SOTA baselines in capturing the non-seasonal rise of wILI due to contamination by COVID-19 related issues. (a) Showcases the forecasting performance for 1 week ahead forecasting. We notice that CALI-NET outperforms all baselines in 10 out of 11 regions and is in the top 2 in the remaining region (i.e., region 6). Specifically, in region 6, where the CALI-NET model is outperformed by DeltaDensity, further inspection revealed that the un-seasonal peak of the COVID-ILI, was shifted and occurred only after period T_1 (i.e., after the period being modeled here) hence following a more traditional pattern of decaying wILI in T_1 . Despite this, we notice that CALI-NET is very close to the performance of DeltaDensity for region 6. (b) Showcases the forecasting performance for 2 week ahead forecasting. We notice that CALI-NET outperforms all baselines in 7 out of 11 regions and is one of the top two best performing models in 10 regions.

2. **CALI-NET w/o Laplacian:** Here, CALI-NET is trained with a variant of CAEM where the Laplacian regularization is deactivated.
3. **CALI-NET w/o Regional Recon.:** Here, CALI-NET is trained with a variant of CAEM where the effect of the regional reconstruction term is deactivated.

Comparing the performance of CALI-NET to the variant CALI-NET w/o GRU characterizes the effect of recurrence on the wILI forecasting task. We notice an order of magnitude degradation in wILI forecasting performance from Table. 2 if a recurrent architecture (namely GRU) is excluded from CAEM. Similarly, a performance comparison between CALI-NET and the variant CALI-NET w/o Laplacian characterizes the effect of the Laplacian regularization (i.e., the ability of CAEM to model region inter-dependencies). We notice that CALI-NET outperforms the variant without Laplacian regularization (CALI-NET w/o Laplacian) in 8 out of 11 regions and achieves an average performance improvement of **4.18%**. Finally, we also tested the performance of a variant of CALI-

NET sans the regional reconstruction facet. We notice from Table. 2, that removal of the effect of explicit regional reconstruction (i.e., the regional embedding part of CAEM), also leads to a degradation in performance. Specifically, CALI-NET outperforms the variant without regional reconstruction (CALI-NET w/o Regional Recon.) by **2.23%**.

The robustness of our method with respect to its parameters is characterized in Fig. 8. It is clear that CALI-NET RMSE performance is stable across different selected values of hyperparameters.

A5: EPIDEEP-CN: Further Details

EPIDEEP was designed to incorporate the wILI seasonal curve from the start of a season until week $t - 1$, to predict values for future weeks. In our case, to enable more focused modeling and to deal with data paucity of the currently evolving COVID-ILI season, we modified the original EPIDEEP architecture to map a window of the past W weeks (i.e., weeks $\{t - 1 - W, \dots, t - 1\}$) of wILI values from the current

Table 2: Per-region RMSE performance characterization of the CALI-NET model when different components of CAEM architecture are deactivated.

| Regions | Our Method | CALI-NET w/o GRU | CALI-NET w/o Laplacian | CALI-NET w/o Regional Recon. |
|----------|---------------|------------------|------------------------|------------------------------|
| R1 | 0.9196 | 22.0574 | 0.9118 | 0.9161 |
| R2 | 2.6869 | 9.2662 | 2.6843 | 2.6977 |
| R3 | 1.293 | 13.2952 | 1.3647 | 1.2965 |
| R4 | 1.6605 | 6.9054 | 1.7944 | 1.7345 |
| R5 | 1.5879 | 16.1975 | 1.687 | 1.6532 |
| R6 | 2.93 | 7.8045 | 3.0516 | 2.951 |
| R7 | 2.2805 | 5.7593 | 2.4184 | 2.322 |
| R8 | 1.3774 | 14.9026 | 1.4898 | 1.3949 |
| R9 | 1.8225 | 4.7056 | 1.8099 | 1.8714 |
| R10 | 1.2069 | 6.2994 | 1.2578 | 1.2262 |
| National | 1.3308 | 9.9319 | 1.4597 | 1.4141 |

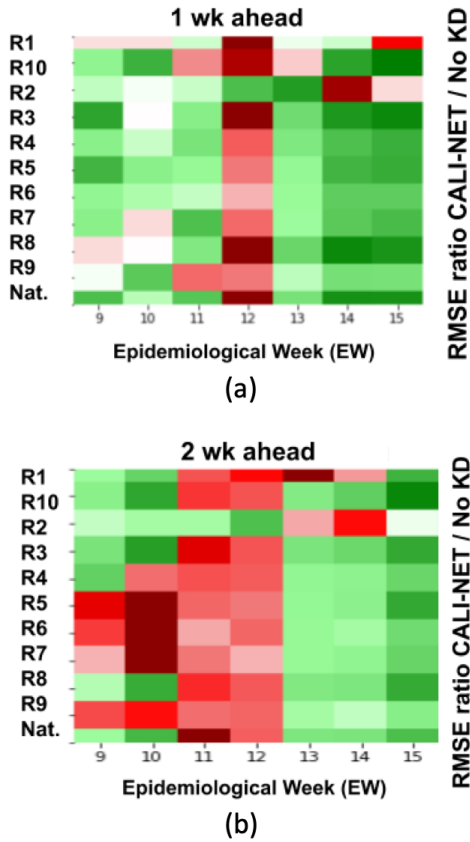


Figure 6: KD Losses 1,2 week ahead predictions. We notice that in the two week ahead forecasts, the variant of CALI-NET without KD losses performs better for EW 11,12 which is due to the season reverting back to typical behavior. Overall, CALI-NET with KD losses performs better than the variant without KD losses for a majority of the cases.

season to $W + 1$ weeks (i.e. weeks $\{t - 1 - W, \dots, t\}$). We name this new architecture EPIDEEP-CN (EPIDEEP-CALI-

NET). The previous EPIDEEP architecture was designed to have multiple regional models, each trained on data for a single region. In EPIDEEP-CN, to leverage inter-regional dependencies, we train a single model for wILI forecasting across all regions.

A6: Description of COVID-Related Exogenous Data

In this section, we describe in more detail the COVID-related signals presented in Table 1 of the main paper. Note that all our signals are captured weekly.

1. *Confirmed cases*: New confirmed COVID-19 cases.
2. *ICU beds*: Number of people who have gone into the intensive care unit (ICU) for COVID-19.
3. *Hospitalizations*: Number of people who have been hospitalized for COVID-19.
4. *People on ventilation*: Number of people who have been under ventilation due to COVID-19.
5. *Recovered*: Number of people who have recovered from COVID-19.
6. *Deaths*: Number of people who have died due to COVID-19.
7. *Hospitalization rate*: COVID-19-Associated hospitalization rate per 100,000 people surveyed by CDC’s surveillance network.
8. *ILI ER visits*: Emergency room visits due to influenza-like illnesses.
9. *CLI ER visits*: Emergency room visits due to COVID-like illnesses.
10. *People tested*: Total number of people tested for COVID-19.
11. *Negative cases*: Total number of people whose tests for COVID-19 resulted negative.
12. *Emergency facilities reporting*: Total number of emergency facilities reporting to CDC the following signals: ILI ER visits and CLI ER visits.

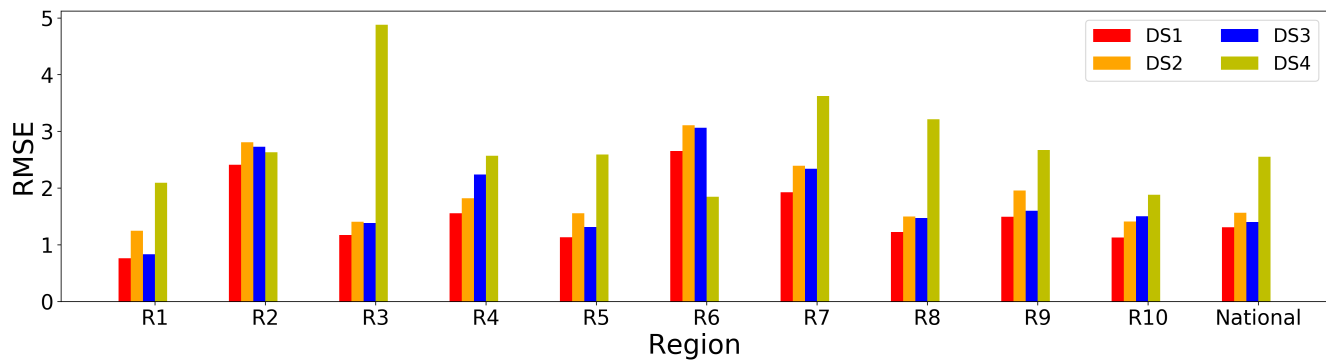


Figure 7: We conduct an experiment to characterize, per region, the usefulness of each broad type of COVID-related data signals. Each bar in the plot indicates the forecasting RMSE per region when CALI-NET only uses data from a single bucket.

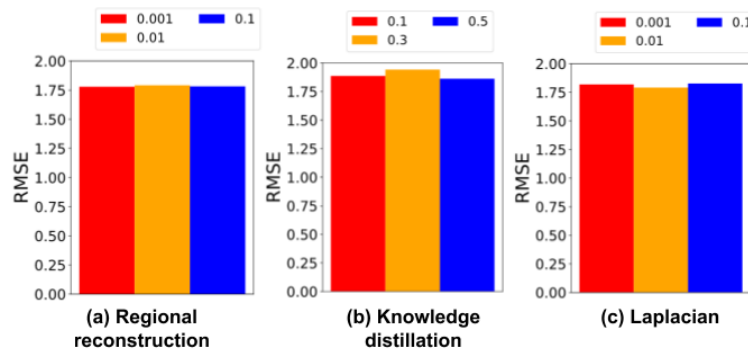


Figure 8: Overall RMSE for CALI-NET while varying its most important hyperparameters. (a) Weight of regional reconstruction loss. (b) Weight of knowledge distillation loss α . (c) Weight of Laplacian regularization loss.

13. *No. of providers*: Total number of health care providers (facilities) reporting ILI counts to CDC.
14. *Digital thermometer readings*: Aggregated and anonymized data from influenza-like illness linked to fever provided by Kinsa (Miller et al. 2018). Collected via crowdsourcing from digital thermometers and accompanying mobile applications.
15. *Health related tweets*: A measure of the percentage of tweets indicating influenza symptoms with method described in (Dredze et al. 2014).